JACS
JOURNAL OF THE AMERICAN CHEMICAL SOCIETY
Communication
pubs.acs.org/JACS

Isomerism in $Au_{28}(SR)_{20}$ Nanocluster and Stable Structures

Yuxiang Chen,[†] Chong Liu,[‡] Qing Tang,[§] Chenjie Zeng,[†] Tatsuya Higaki,[†] Anindita Das,[†] De-en Jiang,*[,§] Nathaniel L. Rosi,[‡] and Rongchao Jin*[,†]

[†]Department of Chemistry, Carnegie Mellon University, Pittsburgh, Pennsylvania 15213, United States
[‡]Department of Chemistry, University of Pittsburgh, Pittsburgh, Pennsylvania 15213, United States
[§]Department of Chemistry, University of California, Riverside, California 92521, United States

Supporting Information

ABSTRACT: Understanding the isomerism phenomenon at the nanoscale is a challenging task because of the prerequisites of precise composition and structural information on nanoparticles. Herein, we report the ligand-induced, thermally reversible isomerization between two thiolate-protected 28-gold-atom nanoclusters, i.e. $Au_{28}(S\text{-}c\text{-}C_6H_{11})_{20}$ (where -*c*-C_6H_{11} = cyclohexyl) and $Au_{28}(SPh\text{-}^tBu)_{20}$ (where -Ph-^{t}Bu = 4-*tert*-butylphenyl). The intriguing ligand effect in dictating the stability of the two $Au_{28}(SR)_{20}$ structures is further investigated via dispersion-corrected density functional theory calculations.

Isomerism is one of the important phenomena in molecular sciences and commonly observed in organic chemistry, in which the molecules with the same formula exhibit a different organization of atoms. Such a variation leads to distinct differences in physical and chemical properties of the isomers, which remarkably enhances the diversity of organic compounds; thus, the concept of isomerism is of fundamental importance at the molecular scale. An interesting question is whether isomerism also exists at the nanoscale. Can one observe the isomerization process in a nanoparticle? If so, how can one control such a process? In order to address these fundamental questions, two prerequisites should first be met. One is to identify the precise composition of the nanoparticle, and the other is to determine the total structure (including the core and surface ligands) of the nanoparticle. Recent progress in the synthesis, structural characterization, and theoretical studies of atomically precise noble metal nanoclusters (1−2 nm)[1−15] has opened up exciting opportunities for studying the isomerism phenomenon at the nanoscale.

In atomically precise gold nanoclusters, the commonly observed isomerism is the stereoisomerism, i.e., the optical isomerism of chiral gold nanoclusters.[15,16] The separation of left- and right-handed isomers gives rise to chiroptical activity.[15,16c,d] On the other hand, structural isomerism in gold nanoclusters is rarely observed except in two cases, i.e. phosphine-protected Au_8 and thiolate-protected Au_{38} nanoclusters.[17,18] For the latter, a low temperature synthetic method was employed to obtain a *metastable* $Au_{38}(SC_2H_4Ph)_{24}$ structure[18] in contrast with the thermodynamically stable biicosahedral $Au_{38}(SC_2H_4Ph)_{24}$.[16b] The metastable Au_{38} isomer was found to *irreversibly* transform into the stable biicosahedral isomer under thermal conditions (e.g., 50 °C),[18] indicating that the low temperature Au_{38} isomer is a kinetically trapped species, and there is only one thermodynamically stable structure thus far for the magic-sized cluster of 38 gold atoms.[16b,19,20] It is worth noting that different $Au_{24}L_{20}$ structures[21] were reported, but different types of ligands (L = thiolate vs selenolate) were involved.

Here we report the discovery of structural isomerism in the $Au_{28}(SR)_{20}$ nanocluster (R= *c*-C_6H_{11} vs Ph-^{t}Bu). A new $Au_{28}(S\text{-}c\text{-}C_6H_{11})_{20}$ structure is determined, which differs from the previously reported $Au_{28}(SPh\text{-}^tBu)_{20}$ counterpart.[16d] Unlike the case of $Au_{38}(SC_2H_4Ph)_{24}$ isomerization,[18] the two Au_{28} nanoclusters are both thermodynamically stable. Interestingly, they can also be *reversibly* transformed into each other through ligand exchange reactions under thermal conditions (e.g., 80 °C). Although the carbon tails of the two thiolate ligands are different, these two Au_{28} isomers have the same number of gold atoms and of thiolate ligands; hence, they constitute quasi-isomers. In fact, the difference between the two thiolate ligands is the driving force for the isomerization process to occur thermally by overcoming the energy barrier between the two stable structures. The observation of such a ligand-induced isomerization process at the nanoscale provides valuable guidance for fundamental investigations of isomerism in nanomaterials.

In a typical experiment, 5 mg of $Au_{28}(SPh\text{-}^tBu)_{20}$ nanocluster was first made[16d] and then reacted with excess cyclohexanethiol (0.5 mL) for 2 h at 80 °C; a new $Au_{28}(S\text{-}c\text{-}C_6H_{11})_{20}$ nanocluster was formed. The reversed process was achieved under similar conditions, i.e., reaction of $Au_{28}(S\text{-}c\text{-}C_6H_{11})_{20}$ nanocluster with excess 4-*tert*-butylbenzenethiol at 80 °C to form the $Au_{28}(SPh\text{-}^tBu)_{20}$ nanocluster as the final product (see Supporting Information for details). The yields of both reactions are >90% (Au atom basis). Single crystal growth of the new $Au_{28}(S\text{-}c\text{-}C_6H_{11})_{20}$ nanocluster was performed via vapor diffusion of pentane into a dichloromethane solution of $Au_{28}(S\text{-}c\text{-}C_6H_{11})_{20}$. Dark orange crystals were observed after ∼3 days. The total structure was solved by single-crystal X-ray diffraction measurements.

The $Au_{28}(S\text{-}c\text{-}C_6H_{11})_{20}$ nanoclusters crystallize in a centrosymmetric space group *P*2/*c*, and the total structure is shown in Figure 1A. It exhibits a prolate shape with quasi-D_2 symmetry. Views from the three mutually perpendicular C_2 axes are shown in the supporting Figure S1. Since there is no mirror plane in the structure, $Au_{28}(S\text{-}c\text{-}C_6H_{11})_{20}$ is chiral as its counterpart, $Au_{28}(SPh\text{-}^tBu)_{20}$.[16d]

Received: November 18, 2015
Published: January 21, 2016

DOI: 10.1021/jacs.5b12094
J. Am. Chem. Soc. 2016, 138, 1482−1485

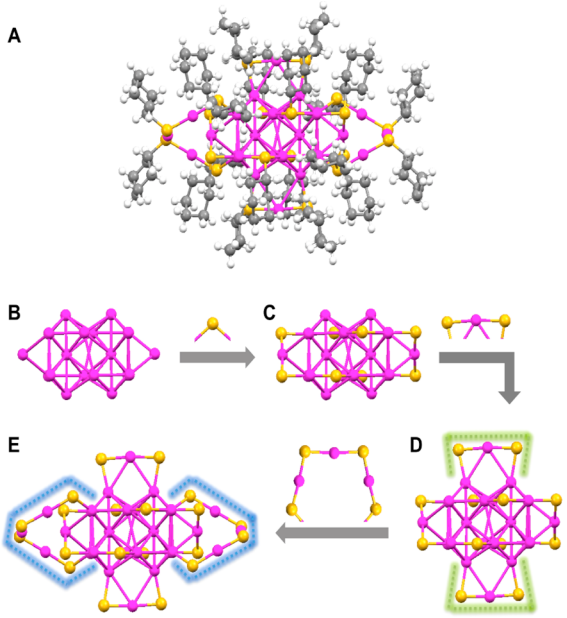

Figure 1. $Au_{28}(S\text{-}c\text{-}C_6H_{11})_{20}$ nanocluster and its structural dissection. (A) Total structure; (B) Au_{20} kernel; (C) Au_{20} kernel capped by eight simple bridging thiolates; (D) Monomeric staples highlighted in green lines; (E) Trimeric staples highlighted in blue lines. Color codes: magenta = gold; orange = sulfur; gray = carbon; white = hydrogen.

Dissection of $Au_{28}(S\text{-}c\text{-}C_6H_{11})_{20}$ is shown in Figure 1B–E. First, it contains a face-centered cubic (FCC) based Au_{20} kernel (Figure 1B), which shows quasi-D_{2h} symmetry. This Au_{20} kernel is capped by eight simple bridging thiolates (Figure 1C). Then, two monomeric staple motifs (SR-Au-SR) are anchored on the top and bottom sides of the Au_{20} kernel, highlighted in green (Figure 1D). Finally, two trimeric staple motifs (SR-Au-SR-Au-SR-Au-SR) protect the left and right sides of the Au_{20} kernel, highlighted in blue (Figure 1E). Of note, Knoppe et al. reported that the eight bridging thiolates in $Au_{28}(SPh\text{-}^tBu)_{20}$ could be viewed as two trimetric staple motifs.[22] We have provided this alternative view for $Au_{28}(S\text{-}c\text{-}C_6H_{11})_{20}$ (Figure S2) based on the atomic charge distribution (Table S1).

In order to better illustrate the differences between $Au_{28}(S\text{-}c\text{-}C_6H_{11})_{20}$ and $Au_{28}(SPh\text{-}^tBu)_{20}$, we provide a detailed structural comparison from the inner gold kernel to the gold–sulfur interface (Figure 2). Both Au_{28} isomers show an FCC-based Au_{20} kernel (Figure 2A, C) and have eight bridging thiolates binding

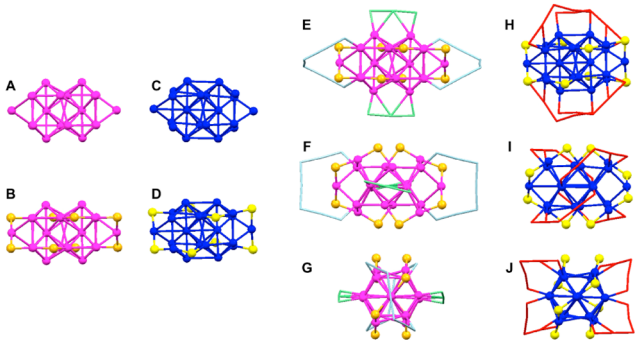

Figure 2. Structural comparison of kernel structures (A-B vs C-D) and surface structures (E-G vs H-J) of $Au_{28}(S\text{-}c\text{-}C_6H_{11})_{20}$ and $Au_{28}(SPh\text{-}^tBu)_{20}$.

to the Au_{20} kernel with the same pattern but exhibiting slightly different distortions (Figure 2B, D). The most distinct difference between these two Au_{28} nanoclusters lies in the gold–sulfur interface, i.e., the arrangement of the remaining "$Au_8(SR)_{12}$" unit on the inner structure. In $Au_{28}(S\text{-}c\text{-}C_6H_{11})_{20}$, the eight gold atoms and 12 thiolate ligands are arranged into two trimeric staples and two monomeric staples (Figure 2E–G), whereas in the $Au_{28}(SPh\text{-}^tBu)_{20}$ the eight gold atoms and 12 thiolate ligands are arranged into four dimeric staples (Figure 2H–J).

A comparison of bond lengths of Au–Au, Au–S, and S–C between the two Au_{28} nanoclusters is provided in the supporting Table S2. The average Au–Au bond length in the Au_{20} kernel of $Au_{28}(S\text{-}c\text{-}C_6H_{11})_{20}$ (3.03 Å) is longer than that in $Au_{28}(SPh\text{-}^tBu)_{20}$ (2.98 Å) by 1.7%. Moreover, the average $Au_{(staple)}$–$Au_{(kernel)}$ bond length also has a 2.8% elongation in the $Au_{28}(S\text{-}c\text{-}C_6H_{11})_{20}$ (3.34 Å) compared to $Au_{28}(SPh\text{-}^tBu)_{20}$ (3.25 Å). The Au–S bond length in the $Au_{28}(S\text{-}c\text{-}C_6H_{11})_{20}$ nanocluster is almost the same as that in the $Au_{28}(SPh\text{-}^tBu)_{20}$ nanocluster (2.32 Å vs 2.31 Å). The longer average S–C bond length (3.4%) in $Au_{28}(S\text{-}c\text{-}C_6H_{11})_{20}$ than that in $Au_{28}(SPh\text{-}^tBu)_{20}$ is due to the electronic conjugation effect in aromatic thiolate ligands.

The overall structural expansion of the $Au_{28}(S\text{-}c\text{-}C_6H_{11})_{20}$ nanocluster as compared to the $Au_{28}(SPh\text{-}^tBu)_{20}$ nanocluster and their surface-staple differences are also reflected in the optical spectra. Although these two Au_{28} quasi-isomers show similar spectral profiles, large blue shifts of the absorption peaks in $Au_{28}(S\text{-}c\text{-}C_6H_{11})_{20}$ can be easily seen (Figure 3A). Specifically,

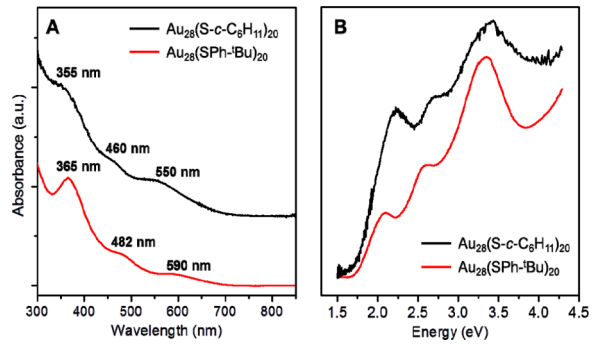

Figure 3. (A) Optical spectra of $Au_{28}(S\text{-}c\text{-}C_6H_{11})_{20}$ (black profile) and $Au_{28}(SPh\text{-}^tBu)_{20}$ (red); (B) Photon-energy plot.

the two absorption peaks at 590 and 482 nm in the $Au_{28}(SPh\text{-}^tBu)_{20}$ nanocluster blue shift to 550 and 460 nm respectively in the $Au_{28}(S\text{-}c\text{-}C_6H_{11})_{20}$ nanocluster. In addition, the 365 nm absorption peak in $Au_{28}(SPh\text{-}^tBu)_{20}$ becomes less prominent in $Au_{28}(S\text{-}c\text{-}C_6H_{11})_{20}$ and blue shifts to 355 nm. These spectral differences are more readily found in the photon energy plots (Figure 3B). By extrapolating the absorbance to zero, both $Au_{28}(SR)_{20}$ isomers have a similar HOMO–LUMO gap (~1.7 eV); this is due to the similar Au_{20} kernel, which dictates the optical spectrum to a large extent.

Interestingly, the two isomeric structures can be reversibly transformed via thermal ligand exchange. We monitored the reation processes by UV–vis spectroscopy. When $Au_{28}(SPh\text{-}^tBu)_{20}$ reacts with excess cyclohexanethiol at 80 °C for 10 min (Figure S3A), the two absorption bands at 590 and 482 nm blue shift to 550 and 460 nm, respectively, and the peak at 365 nm becomes less prominent. To ensure the completion of the transformation to $Au_{28}(S\text{-}c\text{-}C_6H_{11})_{20}$, the reaction was allowed to proceed for 2 h. No byproducts were observed. The rapid formation of $Au_{28}(S\text{-}c\text{-}C_6H_{11})_{20}$ nanocluster suggests an

DOI: 10.1021/jacs.5b12094
J. Am. Chem. Soc. 2016, 138, 1482–1485

associative mechanism that is similar to the reported ligand exchange on thiolate-protected gold nanoclusters.[13] The reversed process can also be triggered by thermal ligand exchange of $Au_{28}(S\text{-}c\text{-}C_6H_{11})_{20}$ with excess 4-*tert*-butylbenzenethiol at 80 °C (Figure S3B). The peaks at 590, 482, and 365 nm are indicative of the formation of $Au_{28}(SPh\text{-}^tBu)_{20}$. This ligand-induced reversible isomerism in the two $Au_{28}(SR)_{20}$ nanoclusters provides important insights into the role of surface-protecting ligands in dictating the stable structure of magic-sized gold nanoclusters.

Previous research has reported the intriguing role of surface-protecting ligands in determining the structure of gold nanoclusters,[16e,f,23,24] which has culminated in the establishment of a ligand-exchange-induced size/structure transformation (LEIST) methodology for controlling the nanocluster size and structure.[23] In such a process, the structural change is always accompanied by size change, and notable examples include the size transformation of $Au_{144}(SC_2H_4Ph)_{60}$ to $Au_{133}(SPh\text{-}^tBu)_{52}$,[16f] $Au_{38}(SC_2H_4Ph)_{24}$ to $Au_{36}(SPh\text{-}^tBu)_{24}$,[5b] and $Au_{25}(SC_2H_4Ph)_{18}$ to $Au_{28}(SPh\text{-}^tBu)_{20}$.[16d] These size transformation processes seem to preclude an isomerization process with the $Au_n(SR)_m$ formula retained under the harsh conditions of thermal ligand exchange. The introduction of a new type of thiol ligand with special structural features disturbs the initial stable structure with the original ligand. To reach a new thermodynamically favorable structure, the gold nanoclusters often lose or gain gold atoms during the ligand exchange process.[5b] In other words, the pathway of isomerization to a new stable structure is less likely to occur than the LEIST pathway; thus, the discovery of Au_{28} reversible isomerization upon ligand exchange is significant and provides important information about the central question[1]—what determines the stability of nanoclusters? The reversible isomerization between $Au_{28}(S\text{-}c\text{-}C_6H_{11})_{20}$ and $Au_{28}(SPh\text{-}^tBu)_{20}$ reveals that there are two thermodynamically stable states in the magic size of the 28-gold-atom nanocluster. The preference of $Au_{28}(SR)_{20}$ for a specific state or structure depends on the carbon tail of the thiolate ligand, i.e., cyclohexyl vs 4-*tert*-butylphenyl.

To further explain this intriguing phenomenon, we carried out density functional theory (DFT) calculations. The ligand effect on the stability of the two quasi-isomers is investigated via dispersion-corrected DFT computations that incorporate van der Waals (vdW) interactions into the DFT energetics.[12b] As shown in Figure 4 and Table S3, both experimental structures, $Au_{28}(S\text{-}c\text{-}C_6H_{11})_{20}$ (labeled as α in Figure 4A) and $Au_{28}(SPh\text{-}^tBu)_{20}$ (labeled as β in Figure 4C), are indeed thermodynamically stable. The energy preference of the α structure is 0.76 eV in the case of the cyclohexanethiolate ligand. The energy preference of the β structure is 0.71 eV when the 4-*tert*-butylbenzenethiolate ligand is used. By breaking down the total energy into DFT and vdW contributions, we found that, for $Au_{28}(S\text{-}c\text{-}C_6H_{11})_{20}$, the preference for the α structure (Figure 4A) over the β structure (Figure 4B) is largely due to the much lower DFT energy (by 1.72 eV) which overwhelms the penalty in the vdW interaction (higher by 0.96 eV). On the other hand, for $Au_{28}(SPh\text{-}^tBu)_{20}$, the preference for the β structure (Figure 4C) over the α structure (Figure 4D) mainly arises from the more favorable vdW interaction of the packing ligands (by 0.57 eV); the DFT energy between them is close (by 0.14 eV).

Another interesting question arises—why does such ligand-induced isomerism not occur in $Au_{36}(SR)_{24}$ (R = Ph-^{t}Bu vs *c*-C_5H_9)? One possible answer may be due to the nanocluster symmetry. In the rod-shaped Au_{28} system, the two quasi-isomers share the same D_2 symmetry, which means that the nanocluster

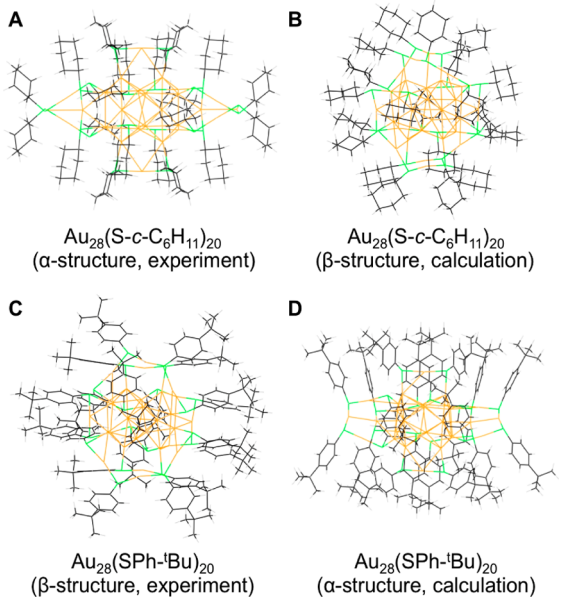

Figure 4. Optimized structures of the four possible $Au_{28}(SR)_{20}$ quasi-isomers.

could still preserve its symmetry after isomerization. However, in the tetrahedral Au_{36} system, there is no way for simple rearrangement of surface-protecting motifs to achieve a new structure which could maintain the same D_{2d} symmetry. This might explain why different ligands all result in the same stable Au_{36} structure.[1a]

The surface structure of nanoparticles plays a pivotal role in catalysis. Since the two Au_{28} nanoclusters have the same Au_{20} kernel but different surface structures, they may serve as an ideal system to test the surface structural influence on the catalytic properties. We choose the catalytic CO oxidation as a probe reaction. The two Au_{28} nanoclusters (0.32 μmol for each) were respectively deposited onto 500 mg CeO_2 supports via wet deposition, followed by O_2 pretreatment at 150 °C for 1 h (note: no ligand desorbs below 200 °C) and then cooling to room temperature (see Supporting Information for details). In the catalytic test, the $Au_{28}(S\text{-}c\text{-}C_6H_{11})_{20}$ nanocluster indeed exhibits higher catalytic activity toward CO oxidation than does the $Au_{28}(SPh\text{-}^tBu)_{20}$ nanocluster (black vs red curves in Figure 5A). We rationalize that the surface structure in $Au_{28}(S\text{-}c\text{-}C_6H_{11})_{20}$ is more accessible compared with the $Au_{28}(SPh\text{-}^tBu)_{20}$ nanocluster due to the more protruded staple motifs and the less steric hindrance for the former. The CO adsorption sites were found to

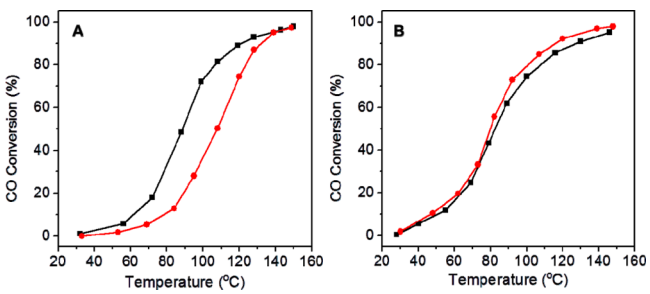

Figure 5. CO oxidation light-off curves of CeO_2 supported $Au_{28}(S\text{-}c\text{-}C_6H_{11})_{20}$ (black profile) and $Au_{28}(SPh\text{-}^tBu)_{20}$ (red) catalysts. (A) Catalysts pretreated with O_2 at 150 °C for 1 h; (B) pretreated with O_2 at 300 °C for 1 h to remove ligands.

DOI: 10.1021/jacs.5b12094
J. Am. Chem. Soc. 2016, 138, 1482−1485

be on the staple Au atoms for both Au_{28} nanoclusters via DFT modeling (Figure S4). When the catalysts were pretreated with O_2 at 300 °C (above ligand desorption temperature) for 1 h to remove the thiolate ligands, the difference in catalytic activity disappeared (Figure 5B). We note that, after the removal of ligands, the remaining bare gold clusters may rearrange into a similar structure since the structure-directing role of ligands is no longer present; this explains the similar catalytic activity of the ligand-off clusters. This observation explicitly demonstrates the surface effect of the two Au_{28} isomers.

In summary, ligand-induced reversible isomerization between two thiolate-protected Au_{28} nanoclusters is demonstrated in this work. The two stable $Au_{28}(SR)_{20}$ quasi-isomers (R = Ph-^{t}Bu vs *c*-C_6H_{11}) possess the same Au_{20} kernel but distinctly different surface structures. The origin of reversible isomerization lies in the thiolate ligand's carbon tail structure, which is found to dictate the specific isomer's stability, as revealed by DFT calculations of energies. The different surface structures of the two Au_{28} isomers render different catalytic properties. Future work on the nanoscale isomerism is expected to further advance the fundamental science and practical applications.

■ ASSOCIATED CONTENT

Supporting Information

The Supporting Information is available free of charge on the ACS Publications website at DOI: 10.1021/jacs.5b12094.

Details of the synthesis, crystallization, X-ray analysis, DFT calculations, catalysis, and supporting Figures S1−S4 and Tables S1−S8 (PDF)

Crystallographic data for Au_{28}(S-*c*-C_6H_{11})$_{20}$ (CIF)

■ AUTHOR INFORMATION

Corresponding Authors

*rongchao@andrew.cmu.edu

*de-en.jiang@ucr.edu

Notes

The authors declare no competing financial interest.

■ ACKNOWLEDGMENTS

The work is supported by the Air Force Office of Scientific Research under AFOSR Award No. FA9550-11-1-9999 (FA9550-11-1-0147) and the Camille Dreyfus Teacher-Scholar Awards Program. DFT computation was supported by University of California, Riverside.

■ REFERENCES

(1) (a) Jin, R. *Nanoscale* **2015**, *7*, 1549. (b) Qian, H.; Zhu, M.; Wu, Z.; Jin, R. *Acc. Chem. Res.* **2012**, *45*, 1470.

(2) Wang, Y.; Su, H.; Xu, C.; Li, G.; Gell, L.; Lin, S.; Tang, Z.; Häkkinen, H.; Zheng, N. *J. Am. Chem. Soc.* **2015**, *137*, 4324.

(3) Niihori, Y.; Kikuchi, Y.; Kato, A.; Matsuzaki, M.; Negishi, Y. *ACS Nano* **2015**, *9*, 9347.

(4) Takano, S.; Yamazoe, S.; Koyasu, K.; Tsukuda, T. *J. Am. Chem. Soc.* **2015**, *137*, 7027.

(5) (a) Chen, Y.; Zeng, C.; Kauffman, D. R.; Jin, R. *Nano Lett.* **2015**, *15*, 3603. (b) Zeng, C.; Liu, C.; Pei, Y.; Jin, R. *ACS Nano* **2013**, *7*, 6138.

(6) Wan, X.-K.; Tang, Q.; Yuan, S.-F.; Jiang, D.-e.; Wang, Q.-M. *J. Am. Chem. Soc.* **2015**, *137*, 652.

(7) Yuan, X.; Zhang, B.; Luo, Z.; Yao, Q.; Leong, D. T.; Yan, N.; Xie, J. *Angew. Chem., Int. Ed.* **2014**, *53*, 4623.

(8) Zeng, C.; Chen, Y.; Li, G.; Jin, R. *Chem. Mater.* **2014**, *26*, 2635.

(9) Wang, D.; Padelford, J. W.; Ahuja, T.; Wang, G. *ACS Nano* **2015**, *9*, 8344.

(10) Pyo, K.; Thanthirige, V. D.; Kwak, K.; Pandurangan, P.; Ramakrishna, G.; Lee, D. *J. Am. Chem. Soc.* **2015**, *137*, 8244.

(11) AbdulHalim, L. G.; Bootharaju, M. S.; Tang, Q.; Del Gobbo, S.; AbdulHalim, R. G.; Eddaoudi, M.; Jiang, D.-e.; Bakr, O. M. *J. Am. Chem. Soc.* **2015**, *137*, 11970.

(12) (a) Jiang, D.-e. *Nanoscale* **2013**, *5*, 7149. (b) Tang, Q.; Ouyang, R.; Tian, Z.; Jiang, D.-e. *Nanoscale* **2015**, *7*, 2225.

(13) Fernando, A.; Aikens, C. M. *J. Phys. Chem. C* **2015**, *119*, 20179.

(14) Pei, Y.; Zeng, X. C. *Nanoscale* **2012**, *4*, 4054.

(15) Knoppe, S.; Bürgi, T. *Acc. Chem. Res.* **2014**, *47*, 1318.

(16) (a) Jadzinsky, P. D.; Calero, G.; Ackerson, C. J.; Bushnell, D. A.; Kornberg, R. D. *Science* **2007**, *318*, 430. (b) Qian, H.; Eckenhoff, W. T.; Zhu, Y.; Pintauer, T.; Jin, R. *J. Am. Chem. Soc.* **2010**, *132*, 8280. (c) Knoppe, S.; Dolamic, I.; Bürgi, T. *J. Am. Chem. Soc.* **2012**, *134*, 13114. (d) Zeng, C.; Li, T.; Das, A.; Rosi, N. L.; Jin, R. *J. Am. Chem. Soc.* **2013**, *135*, 10011. (e) Chen, Y.; Zeng, C.; Liu, C.; Kirschbaum, K.; Gayathri, C.; Gil, R. R.; Rosi, N. L.; Jin, R. *J. Am. Chem. Soc.* **2015**, *137*, 10076. (f) Zeng, C.; Chen, Y.; Kirschbaum, K.; Appavoo, K.; Sfeir, M. Y.; Jin, R. *Sci. Adv.* **2015**, *1*, e1500045. (g) Dass, A.; Theivendran, S.; Nimmala, P. R.; Kumara, C.; Jupally, V. R.; Fortunelli, A.; Sementa, L.; Barcaro, G.; Zuo, X.; Noll, B. C. *J. Am. Chem. Soc.* **2015**, *137*, 4610. (h) Yang, H.; Wang, Y.; Edwards, A. J.; Yan, J.; Zheng, N. *Chem. Commun.* **2014**, *50*, 14325. (i) Zeng, C.; Chen, Y.; Liu, C.; Nobusada, K.; Rosi, N. L.; Jin, R. *Sci. Adv.* **2015**, *1*, e1500425. (j) Zeng, C.; Liu, C.; Chen, Y.; Rosi, N. L.; Jin, R. *J. Am. Chem. Soc.* **2014**, *136*, 11922. (k) Schaaff, T. G.; Whetten, R. L. *J. Phys. Chem. B* **2000**, *104*, 2630.

(17) Kamei, Y.; Shichibu, Y.; Konishi, K. *Angew. Chem., Int. Ed.* **2011**, *50*, 7442.

(18) Tian, S.; Li, Y.-Z.; Li, M.-B.; Yuan, J.; Yang, J.; Wu, Z.; Jin, R. *Nat. Commun.* **2015**, *6*, 8667.

(19) Pei, Y.; Gao, Y.; Zeng, X. C. *J. Am. Chem. Soc.* **2008**, *130*, 7830.

(20) Lopez-Acevedo, O.; Tsunoyama, H.; Tsukuda, T.; Häkkinen, H.; Aikens, C. M. *J. Am. Chem. Soc.* **2010**, *132*, 8210.

(21) (a) Das, A.; Li, T.; Li, G.; Nobusada, K.; Zeng, C.; Rosi, N. L.; Jin, R. *Nanoscale* **2014**, *6*, 6458. (b) Song, Y.; Wang, S.; Zhang, J.; Kang, X.; Chen, S.; Li, P.; Sheng, H.; Zhu, M. *J. Am. Chem. Soc.* **2014**, *136*, 2963. (c) Pei, Y.; Pal, R.; Liu, C.; Gao, Y.; Zhang, Z.; Zeng, X. C. *J. Am. Chem. Soc.* **2012**, *134*, 3015.

(22) Knoppe, S.; Malola, S.; Lehtovaara, L.; Bürgi, T.; Häkkinen, H. *J. Phys. Chem. A* **2013**, *117*, 10526.

(23) Zeng, C.; Chen, Y.; Das, A.; Jin, R. *J. Phys. Chem. Lett.* **2015**, *6*, 2976.

(24) (a) Nishigaki, J.-i.; Yamazoe, S.; Kohara, S.; Fujiwara, A.; Kurashige, W.; Negishi, Y.; Tsukuda, T. *Chem. Commun.* **2014**, *50*, 839. (b) Nishigaki, J.-i.; Tsunoyama, R.; Tsunoyama, H.; Ichikuni, N.; Yamazoe, S.; Negishi, Y.; Ito, M.; Matsuo, T.; Tamao, K.; Tsukuda, T. *J. Am. Chem. Soc.* **2012**, *134*, 14295.

DOI: 10.1021/jacs.5b12094
J. Am. Chem. Soc. 2016, 138, 1482−1485